

Flip-Avoiding Interpolating Surface Registration for Skull Reconstruction

Shudong Xie and Wee Kheng Leow

Dept. of Computer Science, National University of Singapore

Computing 1, 13 Computing Drive, Singapore 117417 Email: xshudong, leowwk@comp.nus.edu.sg

Abstract—Reconstruction of skulls from defective models is a very important and challenging task in craniofacial surgery, forensics, and anthropology. Existing methods typically reconstruct approximating surfaces that regard corresponding points on the target skull as soft constraints, thus incurring non-zero error even for non-defective parts and high overall reconstruction error. This paper proposes a novel method that non-rigidly registers an interpolating surface that regards corresponding target points as hard constraints, thus achieving low reconstruction error. To overcome the shortcoming of interpolating surface, a flip-avoiding method is used to detect and exclude conflicting hard constraints that would otherwise cause surface patches to flip. Comprehensive test results show that our method is more accurate than existing methods and it is robust against severe outliers such as radiation artifacts in CT due to dental implants.

I. INTRODUCTION

3D models of human skulls are very important in craniofacial surgery, forensics, and anthropology. They are often incomplete, fractured, or deformed due to impact injury, criminal acts, or natural processes. Although human skulls have the same global structure, they differ in shape details across age, race and gender. Therefore, reconstruction of normal skulls from defective models is very important and challenging.

Existing skull reconstruction methods can be grouped into three categories: symmetry-based, statistical, and geometric. Symmetry-based methods [1], [2], [3] reflect the non-defective parts on one side of a skull about the mid-plane and regard the reflected model as an estimate of the normal shape of the defective parts on the other side. Due to the natural asymmetry of human skulls [4], the reflected model's surface would not flush with the normal parts on the defective side of the skull, producing surface discontinuities. These methods are not applicable when both sides of a skull are defective.

Statistical methods such as active shape model [5], [6], [7] build a statistical model from a set of normal training skulls. Given a target skull, they compute the model parameters that best fit the non-defective parts of the target, and generate the reconstructed skull from the best-fitting model parameters. To capture all the essential variations in normal human skulls across age, race, and gender, a large number ($\gg 50$) of training skulls is required. The lack of such a large training set has hindered their applications to skull reconstruction.

Geometric methods [8], [9], [10], [11] perform non-rigid registration of a single reference model to fit the non-defective parts of the target model, and regard the registered reference

model as the reconstructed model. The accuracy of geometric methods depends critically on the amount of corresponding points used in non-rigid registration. Methods that use a small set of manually marked landmarks [8], [9], [10] cannot achieve high accuracy. Thus, some methods automatically detect more corresponding points [11].

Non-rigid registration methods can be grouped into two broad categories based on the goal of registration: approximation and interpolation. Methods that produce **approximating surfaces** such as piecewise rigid registration [12] and non-rigid ICP [13], [14] fit a reference surface to the target by minimizing the distance between corresponding reference and target surfaces. They regard the positional correspondence as **soft constraints**, and their registered surfaces have non-zero distance or error to the target surfaces. On the other hand, methods that produce **interpolating surfaces** such as thin-plate spline [15] and Laplacian deformation [16] fit the reference surface to pass through the corresponding target points. They regard the positional correspondence as **hard constraints**, and thus, their registered surfaces have zero error with respect to the corresponding target points.

Among the interpolating methods, TPS is the most popular for reconstruction of skulls [8], [9], [10], [11] because it can tolerate noise by imposing surface smoothness constraint through the minimization of surface bending energy. Laplacian deformation preserves local surface curvature and normal, and it has not been used for skull reconstruction.

Interpolating methods can produce flipped surfaces when there are conflicts in the hard constraints. Flipped surfaces cause severe distortion of surface shape (Fig. 1(e, f)), and are very difficult to remove (Section II). Note that surface flipping is a direct consequence of surface interpolation with conflicting hard constraints. Imposing surface smoothness constraint by energy minimization, such as TPS, cannot remove surface flipping (Fig. 1(f)). In contrast, approximating surfaces can avoid surface flipping because they regard the correspondence as soft constraints and are allowed to ignore conflicting constraints. Their shortcoming is the non-zero reconstruction error of the non-defective parts.

This paper proposes a novel method called **FAIS** (Flip-Avoiding Interpolating Surface) that exploits the strength of interpolating surface while overcoming its shortcoming. It avoids surface flipping by detecting and excluding conflicting hard constraints. Such exclusion is affordable when a very dense set of corresponding points is available (Section IV-B).

Thus, FAIS can reconstruct a skull without flipped surfaces and achieve practically zero error for the non-defective parts. It uses Laplacian deformation instead of the more popular TPS because Laplacian deformation runs faster with increasing amount of hard constraints, whereas TPS runs slower.

II. HANDLING SURFACE INTERFERENCE

There are two general approaches for handling surface flipping and self-intersection: (1) detection and resolution, and (2) avoidance. [17] detects self-intersections by examining the deformation result, and resolves self-intersections by rolling back the mesh to the state before deformation and imposing repulsive forces to keep the potentially intersecting surfaces apart. [18] imposes proximity conditions between mesh vertices and detects violations of proximity conditions, whereas [19], [20] detect self-intersections through collision detection, and resolve self-intersections by remeshing.

The methods in [21], [22] avoid self-intersection by imposing injectivity (one-to-one) condition on free-form deformation function. The injectivity condition confines the free-form deformation of mesh to regions that do not have self-intersection. [23], [24] apply diffeomorphic deformation function. A diffeomorphic function and its inverse are both one-to-one and smooth, and it preserves the topology of the mesh after deformation, thus avoiding self-intersection. These methods produce approximating instead of interpolating surfaces.

[25] devises an ingenious quadrilateral mesh that permits easy detection of possible flippings of mesh edges by arranging the mesh vertices into some forms of total ordering. These flippings are removed from the constraint set for mesh deformation, thus avoiding flippings. Unfortunately, it is non-trivial to convert a triangular mesh to the special quadrilateral mesh, limiting the applicability of this method.

Our FAIS is similar in spirit to [25], except FAIS detects possible flippings of triangular faces before deformation, which are removed from the constraint set for mesh deformation. FAIS's advantage is that it can be applied to triangular meshes, and it is conceptually simpler than [25].

III. FLIP-AVOIDING REGISTRATION

A. Overview

FAIS performs non-rigid interpolating registration of a reference model to a defective target model. To achieve the goals discussed in Section I, FAIS applies the following principles:

- 1) FAIS applies automatic correspondence search methods to obtain dense correspondence. It matches the surface characteristics of the reference and the target (Section III-B), which allows FAIS to ignore outliers. Similar techniques are commonly used in existing methods.
- 2) FAIS detects and removes correspondence that may cause surface flipping (Section III-C), thus achieving flip-avoiding reconstruction with interpolating surfaces.
- 3) Correspondence search is a local operation that is not guaranteed to be anatomically accurate. To reduce the risks of wrong correspondence, FAIS adopts an *iterative incremental* approach that deforms the reference model

very slightly in the early iterations (Section III-D). As the reference registers closer to the target in subsequent iterations, the risk of finding wrong correspondence is reduced, and the reference is allowed to deform more.

B. Correspondence Search

FAIS applies two correspondence search methods. The first method is applied in the early iterations of FAIS. It searches for a corresponding mesh vertex \mathbf{p}' on the target T for each mesh vertex \mathbf{p} on the reference F that satisfies the conditions:

- \mathbf{p}' is near enough to \mathbf{p} : $\|\mathbf{p} - \mathbf{p}'\| \leq D_1$, where D_1 is a constant parameter for search range; and
- \mathbf{p}' and \mathbf{p} have similar surface normals that differ by no greater than 10° .

In the current implementation, D_1 is empirically set at 0.5mm.

The second method is applied in the final step. It searches for a corresponding point \mathbf{p}' on the target T for each mesh vertex \mathbf{p} on the reference F , such that

- \mathbf{p}' is \mathbf{p} 's nearest surface point on T , i.e., the nearest intersection of the surface normal at \mathbf{p} with T , and
- $\|\mathbf{p} - \mathbf{p}'\| \leq D_2$, where D_2 is a constant parameter.

D_2 is larger than D_1 but not so large that wrong correspondence is found. In the current implementation, $D_2 = 3\text{mm}$. The second method can find more corresponding points but is less efficient than the first. So, it is used only in the final step.

If a corresponding point \mathbf{p}' is found for \mathbf{p} , then the vector $\mathbf{v}(\mathbf{p}) = \mathbf{p}' - \mathbf{p}$ is the *correspondence vector* of \mathbf{p} . Otherwise, \mathbf{p} has no correspondence vector. The set C of correspondence contains tuples of the form $(\mathbf{p}, \mathbf{p}')$.

C. Flip Avoidance

Surface flipping is caused by the crossing of correspondence vectors that results in the flipping of a surface patch relative to its neighboring surfaces (Fig. 1). There is no surface flipping if the correspondence vectors do not cross. To derive the condition for flip avoidance, consider two points \mathbf{p} and \mathbf{q} on the surface of a mesh. If their correspondence vectors $\mathbf{v}(\mathbf{p})$ and $\mathbf{v}(\mathbf{q})$ meet at the same point, then they form a triangle with the vector $\mathbf{q} - \mathbf{p}$ from \mathbf{p} to \mathbf{q} (Fig. 1(a)). Let $\theta(\mathbf{p}; \mathbf{q})$ denote the angle made by $\mathbf{v}(\mathbf{p})$ and $\mathbf{q} - \mathbf{p}$, and similarly for $\theta(\mathbf{q}; \mathbf{p})$. Then, basic trigonometry states that

$$\|\mathbf{v}(\mathbf{p})\| \cos \theta(\mathbf{p}; \mathbf{q}) + \|\mathbf{v}(\mathbf{q})\| \cos \theta(\mathbf{q}; \mathbf{p}) = \|\mathbf{p} - \mathbf{q}\|. \quad (1)$$

In general, \mathbf{p} and \mathbf{q} do not meet or intersect at a point in 3D space. Then, the left-hand side of Eq. 1 is the sum of the projections of \mathbf{p} and \mathbf{q} on the vector $\mathbf{q} - \mathbf{p}$. If $\|\mathbf{p} - \mathbf{q}\|$ is less than the left-hand side of Eq. 1, $\mathbf{v}(\mathbf{p})$ and $\mathbf{v}(\mathbf{q})$ will cross in 3D space, causing surface flipping (Fig. 1(d-f)). If $\|\mathbf{p} - \mathbf{q}\|$ is greater than the left-hand side, $\mathbf{v}(\mathbf{p})$ and $\mathbf{v}(\mathbf{q})$ will not cross, and there is no flipping (Fig. 1(b, c)).

Let D denote the upper bound on the length of the correspondence vectors: $\|\mathbf{v}(\mathbf{p})\| \leq D, \forall \mathbf{p}$. Then, \mathbf{p} and \mathbf{q} will not cross if

$$\cos \theta(\mathbf{p}; \mathbf{q}) + \cos \theta(\mathbf{q}; \mathbf{p}) < \frac{\|\mathbf{p} - \mathbf{q}\|}{D}. \quad (2)$$

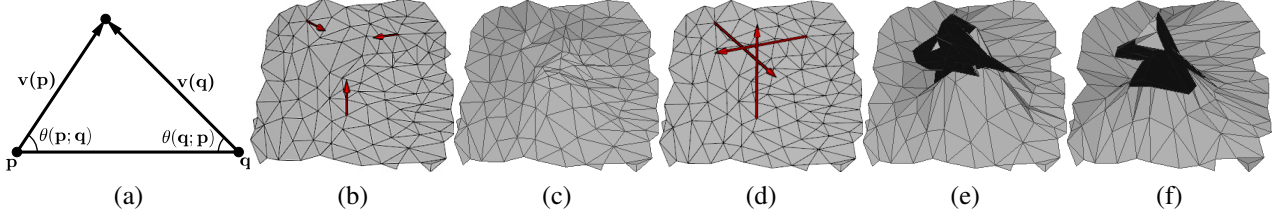


Fig. 1. Surface flipping. (a) Correspondence vectors $\mathbf{v}(\mathbf{p})$ and $\mathbf{v}(\mathbf{q})$ form a triangle with the line joining \mathbf{p} and \mathbf{q} when they meet at the same point. (b) Non-crossing correspondence vectors (arrows) produce (c) no surface flipping. (d) Crossing correspondence vectors cause (e) Laplacian deformation and (f) TPS to produce flipped and distorted surfaces even when they do not intersect. Black regions are surface patches that have flipped.

This condition can be simplified as

$$\cos \theta(\mathbf{p}; \mathbf{q}) < \frac{\|\mathbf{p} - \mathbf{q}\|}{2D} \quad \text{and} \quad \cos \theta(\mathbf{q}; \mathbf{p}) < \frac{\|\mathbf{q} - \mathbf{p}\|}{2D} \quad (3)$$

since Condition 3 implies Condition 2.

In order that $\mathbf{v}(\mathbf{p})$ does not cross any vector $\mathbf{v}(\mathbf{q})$, Condition 3 must be satisfied for all the points \mathbf{q} on the mesh. Since $\cos \theta(\mathbf{p}; \mathbf{q}) \leq 1$, Condition 3 is trivially satisfied for all points \mathbf{q} at a distance larger than $2D$ from \mathbf{p} . Thus, we can state the following conditions for no crossing:

Simple No-Crossing Condition

There is no crossing if, for all pairs $(\mathbf{p}, \mathbf{p}')$ and $(\mathbf{q}, \mathbf{q}')$ in correspondence set C , $\|\mathbf{p} - \mathbf{q}\| > 2D$.

General No-Crossing Condition

There is no crossing if, for each $(\mathbf{p}, \mathbf{p}') \in C$,

$$\begin{aligned} \cos \theta(\mathbf{p}; \mathbf{q}) &< \frac{\|\mathbf{p} - \mathbf{q}\|}{2D}, \\ \forall \mathbf{q} \in N(\mathbf{p}) = \{\mathbf{q} \mid \|\mathbf{p} - \mathbf{q}\| \leq 2D\} \quad \text{and} \quad (\mathbf{q}, \mathbf{q}') \in C. \end{aligned} \quad (4)$$

The simple condition is a special case of the general condition.

D. Reconstruction Algorithm

FAIS reconstructs the resultant model R given a reference model F , a target model T , and known correspondence C^* . C^* is obtained from manual marking of significant anatomical landmarks on F and T that are adequately separated to ensure no crossing. In addition, F and T are assumed to be already spatially aligned by an appropriate algorithm such as fractional ICP [26]. FAIS is summarized in Algorithm 1.

Step 1 non-rigidly registers reference F to target T with known correspondence C^* as the positional constraints, and sets the result R as the registered F . This step matches the overall anatomical shape of R to that of T in order to improve correspondence search in subsequent steps.

Steps 2 to 6 perform K iterations of non-rigid registration in small steps. First, Step 3 finds correspondence C from R to T using the first correspondence search method, which restricts all $\|\mathbf{v}(\mathbf{p})\|$ to be no longer than D_1 (Section III-B). Step 4 chooses a sparse subset C^+ as follows: First, the upper bound D is set to the longest $\|\mathbf{v}(\mathbf{p})\|$ in $C^* \cup C$, thus, $D \leq D_1$. C^+ is initialized with known correspondence C^* . Then, each tuple $(\mathbf{p}, \mathbf{p}')$ in C is checked for sparse distribution: If there is a tuple $(\mathbf{q}, \mathbf{q}')$ in C^+ such that $\|\mathbf{p} - \mathbf{q}\| \leq 2D$, the tuple $(\mathbf{p}, \mathbf{p}')$ is discarded. Otherwise, it is added to C^+ . This step ensures

Algorithm 1: FAIS Flip-Avoiding Interpolating Surface

Input: Reference F , target T , known correspondence C^* .

- 1 Non-rigidly register F to T with positional constraints C^* , and set R as the registered F .
 - 2 **for** k from 1 to K **do**
 - 3 Find correspondence C from R to T using first correspondence search method.
 - 4 Choose a sparse subset C^+ from $C^* \cup C$.
 - 5 Non-rigidly register R to T with constraints C^+ .
 - 6 **end**
 - 7 Find correspondence C from R to T using second correspondence search method.
 - 8 Remove crossings in $C^* \cup C$ giving C^+ .
 - 9 Non-rigidly register R to T with constraints C^+ .
- Output:** Resultant R .
-

that all the reference points in C^+ are separated by a distance greater than $2D$, thereby satisfying the Simple No-Crossing Condition. Step 5 non-rigidly registers R to T , with each \mathbf{p} in C^+ moved by an amount $(k/K)\|\mathbf{v}(\mathbf{p})\|$ along $\mathbf{v}(\mathbf{p})$. Thus, \mathbf{p} is moved toward \mathbf{p}' incrementally, allowing FAIS to recover from possible wrong correspondence in subsequent iterations.

Step 7 finds correspondence C from R to T using the second correspondence search method (Section III-B). Step 8 removes crossings in $C^* \cup C$ as follows: First, the upper bound D is set to the longest $\|\mathbf{v}(\mathbf{p})\|$ in $C^* \cup C$, and the correspondence set C^+ is initialized to C^* . Next, each tuple $(\mathbf{p}, \mathbf{p}')$ in C is checked according to the General No-Crossing Condition. If the condition is satisfied, the tuple is added to C^+ ; otherwise, it is discarded. This step obtains a much denser set of correspondence than the sparse set in Step 4 (Section IV-B). Finally, Step 9 performs the final registration of R to T with C^+ as the positional constraints.

FAIS differs from non-rigid ICP [13], [14], although they have similar iterative structure. Non-rigid ICP performs locally affine registration of approximating surface, whereas FAIS performs non-rigid registration of interpolating surface.

IV. EXPERIMENTS AND DISCUSSIONS

A. Data Preparation and PC Configuration

3D mesh models of skulls were constructed from patients' CT images. A normal skull was randomly selected as the ref-

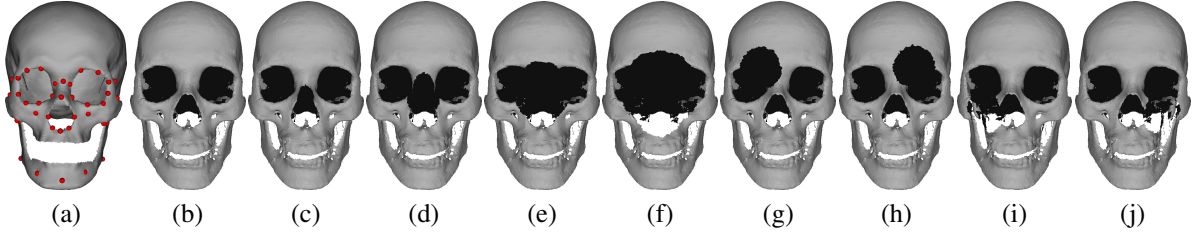


Fig. 2. Sample skull models. (a) Reference model with manual landmarks (red dots). (b) Normal testing skull. (c–f) Synthetic testing skulls with defective parts of different sizes, ranging from radius of 10mm to 40mm. (g–j) Synthetic testing skulls with defective parts at various locations.

reference model (Fig. 2(a)), which had 92550 mesh vertices and 42 manual landmarks. Skull models with much fewer vertices cannot model the surfaces accurately. Teeth in the reference model were omitted because they were less important than facial bones in defining facial appearance, and many patients had missing teeth. Moreover, the resolution of the head CT was insufficient for constructing skull models with sufficient resolution for modeling each tooth accurately. Twenty normal skulls were used for testing. Five of the normal testing skulls were each used to synthesize 8 defective testing skulls with missing parts, giving a total of 40 defective testing skulls. For the examples in Fig. 2(c) to 2(f), the defective parts were produced by removing mesh vertices within a spherical region of radius 10mm to 40mm. For the examples in Fig. 2(g) to 2(j), the spherical regions were all 20mm but located at different locations. The 5 normal testing skulls serve as the ground truth.

The programs were implemented in Mathematica which used Intel MKL to solve linear systems. All tests were run on a PC with Intel i7-2600 CPU at 3.4GHz and 8GB RAM.

B. Dense Correspondence

In this experiment, FAIS was tested in turn with Laplacian deformation and TPS as the non-rigid registration method on a normal testing skull. Figure 3(a) shows that FAIS with Laplacian deformation finds more corresponding points than FAIS with TPS. This is because FAIS with Laplacian deformation is more accurate than FAIS with TPS (Section IV-C).

During the iterative stage from Step 2 to 6, up to 90% of the corresponding points are rejected by the Simple No-Crossing condition. At Step 8, FAIS’s General No-Crossing Condition accepts 80% of the mesh vertices, amounting to about 74,000 corresponding points. In comparison, existing methods such as [8], [9], [10], [11] use several tens to hundreds of corresponding points, which are two orders of magnitude smaller than that of FAIS. With comparatively sparser correspondence sets, existing methods cannot achieve reconstruction accuracy as high as FAIS.

Figure 3(b) shows that Laplacian deformation runs faster and TPS runs slower with increasing amount of hard constraints. Moreover, TPS cannot run in Step 9 because its memory requirement exceeds available memory. FAIS’s execution time is roughly proportional to the number of iterations K .

C. Reconstruction Accuracy

Reconstruction accuracy is highly dependent on the amount of correspondence available. To ensure that the methods tested

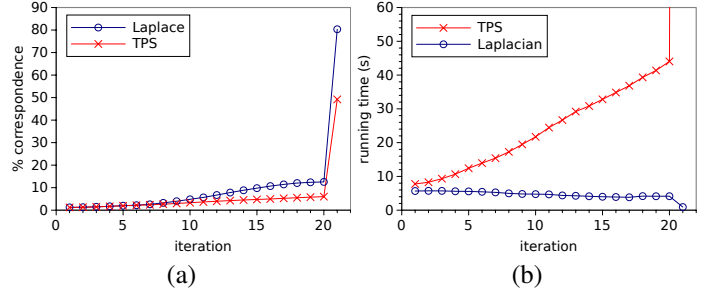


Fig. 3. Correspondence search. (a) Amount of correspondence at various iteration. (b) Running time (sec) is influenced by the amount of correspondence.

have comparable amounts of correspondence, we compare FAIS with existing interpolating surface methods as follows:

- FAIS-1: FAIS with $K = 10$.
- FAIS-2: FAIS with $K = 20$.
- Laplace-1: As Step 1 of FAIS.
- Laplace-2: As Steps 1–6 of FAIS with $K = 1$.
- TPS-1: As Step 1 of FAIS except TPS is used; similar to [8], [9], [10].
- TPS-2: As Steps 1–6 of FAIS with $K = 1$ except TPS is used; similar to [11].

The last four methods are equivalent to FAIS with different steps omitted. TPS-1 and TPS-2 are similar to existing methods, except that existing methods implicitly avoid surface flipping by choosing sparse correspondence sets (Section IV-B).

This test was performed on 20 normal skulls, 40 synthetic defective skulls and 2 real defective skulls. Reconstruction error was measured as the average distance from a mesh vertex on the reconstructed result R to the surface of the ground truth. Besides the overall error E averaged over the testing skulls, errors of the defective parts E_D , non-defective parts with and without positional constraints, respectively E_C and E_N , were measured separately. Some non-defective parts were excluded from the correspondence sets due to flip avoidance, and thus had no positional constraints.

Table I summarizes the reconstruction errors and Fig. 5 details the reconstruction errors for different defective conditions. All methods have zero error E_C for the non-defective parts with positional constraints because they adopt interpolating surfaces and regard positional constraints as hard constraints. E_D is affected by the severity of defects as expected. The error for non-defective parts without correspondence E_N of

TABLE I

AVERAGE RECONSTRUCTION ERRORS OF VARIOUS ALGORITHMS.

E_C , E_N , E_D , and E are, respectively, error (measured in mm) of non-defective parts with positional constraints, non-defective parts without positional constraints, defective parts, and whole skull.

	Normal Skulls			Synthetic Skulls			
	E_C	E_N	E	E_C	E_N	E_D	E
FAIS-1	0.00	1.13	0.32	0.00	1.05	1.00	0.29
FAIS-2	0.00	0.92	0.20	0.00	0.94	1.01	0.22
Laplace-1	0.00	2.97	2.97	0.00	2.97	1.69	2.95
Laplace-2	0.00	2.43	2.39	0.00	2.44	1.60	2.39
TPS-1	0.00	5.46	5.46	0.00	5.63	1.42	5.56
TPS-2	0.00	5.24	5.17	0.00	5.39	1.24	5.26

synthetic testing skulls is in general larger than that of the normal skulls, as expected.

Compared to Laplace and TPS, FAIS has significantly smaller errors E_N for the non-defective parts without positional constraints, and slightly smaller errors E_D for the defective parts. Laplace and TPS have larger E_N than E_D because most of the manual landmarks are placed on the facial bones. Although FAIS-1 runs only half as many iterations as FAIS-2, its error is only slightly larger than that of FAIS-2 and significantly smaller than those of Laplace and TPS. Therefore, FAIS's performance is not significantly affected by the number of iterations K . With FAIS, up to 80% of the reference's vertices have corresponding points that serve as hard constraints, whereas only 10% are available to Laplace and TPS (Section IV-B). Therefore, FAIS has the lowest overall error of $E \leq 0.3\text{mm}$, whereas Laplace and TPS have higher errors of, respectively, $E = 2\text{--}3\text{mm}$ and $E > 5\text{mm}$.

Visual inspection of the reconstructed results for synthetic skulls (Fig. 5(1, 2)) confirms that FAIS's reconstructions are close to the ground truth. On the other hand, the reconstructions of Laplace and TPS have visible errors. Moreover, TPS reconstructions have less accurate aspect ratios.

For the real defective skulls (Fig. 5(3,4)), FAIS's reconstruction of the jaws are close to the targets. Its reconstruction of the missing facial bones are structurally correct but distorted due to the fractured and deformed bones in the targets. The reconstructions of Laplace and TPS appear less distorted because they do not fit the targets closely and are thus closer to the reference (Fig. 2(a)) than the targets.

D. Robustness Against Outliers

CT images that are used to construct 3D skull models can contain radiation artifacts caused by metallic dental implants [27] that are very difficult to remove. Thus, 3D skull models segmented and constructed from CT images often contain metal artifacts (Fig. 6). This test evaluates the robustness of FAIS against outliers such as metal artifacts. The test was performed on 5 actual skulls with metal artifacts. FAIS-2 was tested using two reference models, one without teeth and one

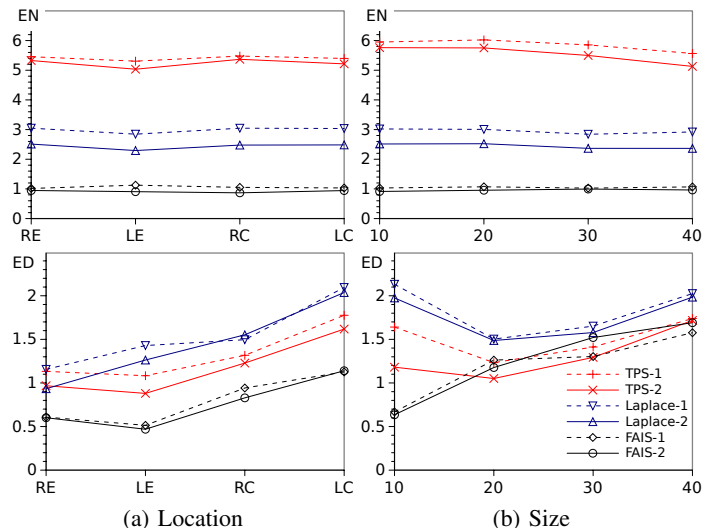


Fig. 4. Reconstruction errors. E_N and E_D are, respectively, error of non-defective parts without positional constraints and error of defective parts. RE: right eye, LE: left eye, RC: right cheek, LC: left cheek.

with teeth. For FAIS-2 with teeth, Step 7 differed slightly such that the first, instead of the second, correspondence search method was applied on the mesh vertices in the teeth region.

Test results show that FAIS-2's correspondence search is robust enough to exclude metal artifacts as possible corresponding points. Consequently, it does not register the reference to the metal artifacts, and the reconstruction is free of metal artifacts. Using reference with teeth, some of the teeth reconstructed by FAIS-2 are slightly distorted because the skull mesh has insufficient resolution to model each tooth accurately. Test results also show that FAIS's reconstruction of the non-defective parts is independent of the reference used, which is expected when an interpolating surface is registered to a large amount of target points that serve as hard constraints.

V. CONCLUSIONS

This paper presented a novel method called FAIS that exploits the strength of a non-rigid registration algorithm with interpolating surface while overcoming its weakness. With interpolating surface that regards positional constraints as hard constraints, FAIS can register a reference model exactly to the corresponding target points of the non-defective parts of a skull, achieving zero reconstruction error for these parts. With flip-avoiding method, conflicting hard constraints are filtered out resulting in flip-free reconstruction. Moreover, FAIS correspondence search methods make it robust against severe outliers such as metal artifacts. Test results also show that FAIS's correspondence set consists of up to 80% of the mesh vertices, which is two orders of magnitude higher than those of existing methods for skull reconstruction. Therefore, FAIS can achieve higher accuracy than existing methods. Its reconstruction accuracy can be affected by severely deformed parts. This shortcoming can be overcome by more accurate detection of deformed parts.

Acknowledgment: This research is supported by MOE grant MOE2014-T2-1-062.

REFERENCES

- [1] L. Cevidanes, S. Tucker, M. Styner, H. Kim, J. C. amd M. Reyes, W. Proffit, T. Turvey, , and M. Jaskolka, "3D Surgical Simulation," *Am J. Orthodontics & Dentofacial Orthopedics*, vol. 138, no. 3, pp. 361–371, 2010.
- [2] E. De Momi, J. Chapuis, I. Pappas, G. Ferrigno, W. Hallermann, A. Schramm, and M. Caversaccio, "Automatic extraction of the mid-facial plane for cranio-maxillofacial surgery planning," *Int. J. Oral and Maxillofacial Surgery*, vol. 35, no. 7, pp. 636–642, 2006.
- [3] L. Wei, W. Yu, M. Li, and X. Li, "Skull assembly and completion using template-based surface matching," in *Proc. Int. Conf. 3D Imaging, Modeling, Processing, Visualization and Transmission*, 2011.
- [4] T. Woo, "On the asymmetry of the human skull," *Biometrika*, vol. 22, no. 3–4, pp. 324–352, 1931.
- [5] M. Lüthi, T. Albrecht, and T. Vetter, "Building shape models from lousy data," in *Proc. MICCAI*, 2009.
- [6] S. Zachow, H. Lamecker, B. Elsholtz, and M. Stiller, "Reconstruction of mandibular dysplasia using a statistical 3D shape model," in *Proc. Computer Assisted Radiology and Surgery*, 2005, pp. 1238–1243.
- [7] K. Zhang, W. K. Leow, and Y. Cheng, "Performance analysis of active shape reconstruction of fractured, incomplete skulls," in *Proc. CAIP*, 2015.
- [8] Q. Deng, M. Zhou, W. Shui, Z. Wu, Y. Ji, and R. Bai, "A novel skull registration based on global and local deformations for craniofacial reconstruction," *Forensic Science Int.*, vol. 208, pp. 95–102, 2011.
- [9] R. J. A. Lapeer and R. W. Prager, "3D shape recovery of a newborn skull using thin-plate splines," *Computerized Medical Imaging & Graphics*, vol. 24, no. 3, pp. 193–204, 2000.
- [10] A. Rosas and M. Bastir, "Thin-plate spline analysis of allometry and sexual dimorphism in the human craniofacial complex," *American J. Physical Anthropology*, vol. 117, pp. 236–245, 2002.
- [11] K. Zhang, Y. Cheng, and W. Leow, "Dense correspondence of skull models by automatic detection of anatomical landmarks," in *Proc. CAIP*, 2013, pp. 229–236.
- [12] F. Bonarrigo, A. Signoroni, and M. Botsch, "Deformable registration using patch-wise shape matching," *Graphical Models*, vol. 76, no. 5, pp. 554–565, 2014.
- [13] B. Amberg, S. Romdhani, and T. Vetter, "Optimal step nonrigid ICP algorithms for surface registration," in *Proc. CVPR*, 2007, pp. 1–8.
- [14] H. Hontani, T. Matsuno, and Y. Sawada, "Robust nonrigid ICP using outlier-sparsity regularization," in *Proc. CVPR*, 2012, pp. 174–181.
- [15] F. L. Bookstein, "Principal warps: Thin-plate splines and the decomposition of deformations," *IEEE Trans. PAMI*, vol. 11, pp. 567–585, 1989.
- [16] O. Sorkine, D. Cohen-Or, Y. Lipman, M. Alexa, C. Rössl, and H. Seidel, "Laplacian surface editing," in *Proc. Eurographics/ACM SIGGRAPH Symp. Geometry Processing*, 2004, pp. 175–184.
- [17] T. McInerney and D. Terzopoulos, "Topology adaptive deformable surfaces for medical image volume segmentation," *IEEE Trans. Medical Imaging*, vol. 18, no. 10, pp. 840–850, 1999.
- [18] J.-O. Lachaud and A. Montanvert, "Deformable meshes with automated topology changes for coarse-to-fine three-dimensional surface extraction," *Medical Image Analysis*, vol. 3, no. 2, pp. 187–207, 1998.
- [19] H. Delingette and J. Montagnat, "Shape and topology constraints on parametric active contours," *Computer Vision and Image Understanding*, vol. 83, no. 2, pp. 140–171, 2001.
- [20] W. Jung, H. Shin, and B. K. Choi, "Self-intersection removal in triangular mesh offsetting," *Computer-Aided Design and Applications*, vol. 1, pp. 477–484, 2004.
- [21] Y. Choi and S. Lee, "Injectivity conditions of 2D and 3D uniform cubic B-spline functions," *Graphical Models*, vol. 62, pp. 411–427, 2000.
- [22] M. Hagenlocker and K. Fujimura, "CFFD: A tool for designing flexible shapes," *The Visual Computer*, vol. 14, 1998.
- [23] A. Khan, E. Aylward, P. Barta, M. Miller, and M. F. Beg, "Semi-automated basal ganglia segmentation using large deformation diffeomorphic metric mapping," in *Proc. MICCAI*, 2005, pp. 238–245.
- [24] X. Zhuang, K. Rhode, S. Arridge, R. Razavi, D. Hill, D. Hawkes, and S. Ourselin, "An atlas-based segmentation propagation framework using locally affine registration—Application to automatic whole heart segmentation," in *Proc. MICCAI*, 2008, pp. 425–433.

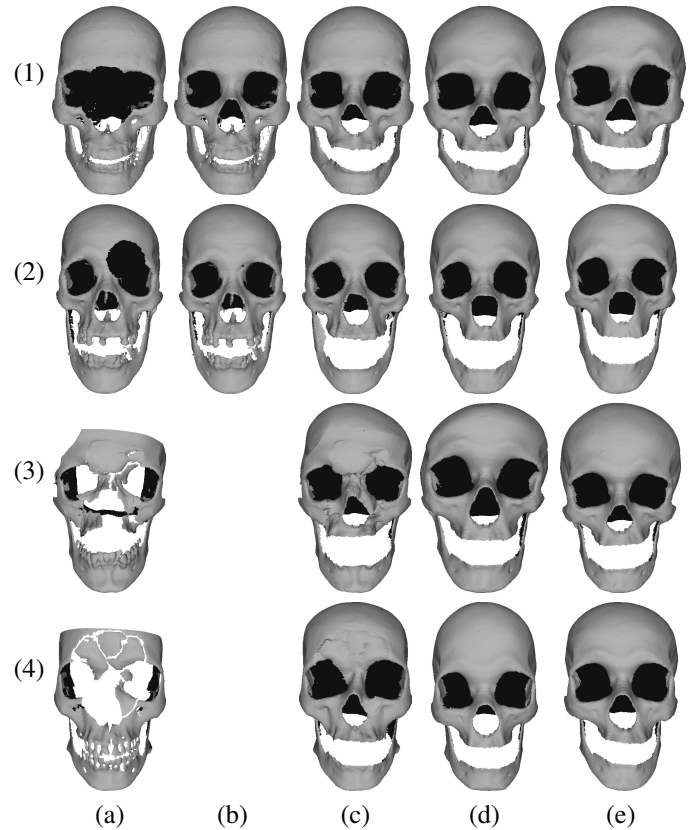


Fig. 5. Sample reconstruction results. (1, 2) Synthetic testing skulls. (3, 4) Real defective skulls. Ground truth is not available. (a) Target, (b) ground truth, (c) FAIS-2, (d) Laplace-2, (e) TPS-2. Results of FAIS-1, Laplace-1, and TPS-1 are similar, and are omitted.

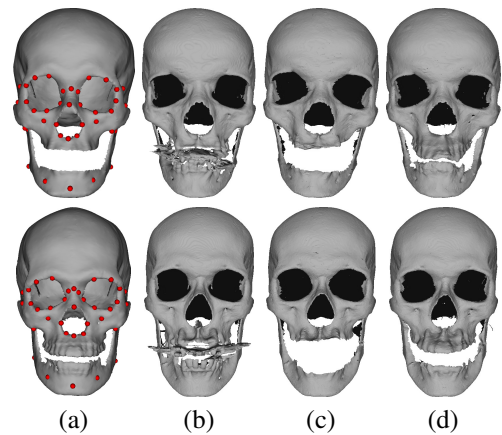


Fig. 6. Robustness against metal artifacts. (a, row 1) Reference without teeth, (a, row 2) reference with teeth, (b) target with metal artifacts, (c) FAIS-2 using reference without teeth, (d) FAIS-2 using reference with teeth.

- [25] F. Ding, W. Yang, W. K. Leow, and S. Venkatesh, "3D segmentation of soft organs by flipping-free mesh deformation," in *Proc. WACV*, 2009.
- [26] J. M. Phillips, R. Liu, and C. Tomasi, "Outlier Robust ICP for Minimizing Fractional RMSD," in *Proc. of Int. Conf. on 3D Digital Imaging and Modeling*, 2007, pp. 427–434.
- [27] A. Mouton, N. Megherbi, K. van Slambrouk, J. Nuyts, and T. P. Breckon, "An experimental survey of metal artefact reduction in computed tomography," *J. X-Ray Science and Tech.*, vol. 21, no. 2, pp. 193–226, 2013.